Author(s): Roschier, Leif & Hakonen, Pertti J. & Bladh, K & Delsing, P. Lehnert, K.W. & Spietz, Lafe & Schoelkopf, Rob

Title: Noise performance of the radio-frequency single-electron transistor

Year: 2004

Version: Final published version

Please cite the original version:

Roschier, Leif & Hakonen, Pertti J. & Bladh, K & Delsing, P. & Lehnert, K.W. & Spietz, Lafe & Schoelkopf, Rob. 2004. Noise performance of the radio-frequency single-electron transistor. Journal of Applied Physics. Volume 95, Issue 3. 1274-1286. ISSN 0021-8979 (printed). DOI: 10.1063/1.1635972

Noise performance of the radio-frequency single-electron transistor

Leif Roschier, P. Hakonen, K. Bladh, P. Delsing, K. W. Lehnert, Lafe Spietz, and R. J. Schoelkopf

Citation: Journal of Applied Physics **95**, 1274 (2004); doi: 10.1063/1.1635972
View online: http://dx.doi.org/10.1063/1.1635972
View Table of Contents: http://scitation.aip.org/content/aip/journal/jap/95/3?ver=pdfcov
Published by the AIP Publishing

Noise performance of the radio-frequency single-electron transistor

Leif Roschier[a] and P. Hakonen
Low Temperature Laboratory, Helsinki University of Technology, P.O. BOX 2200, FIN-02015 HUT, Finland

K. Bladh and P. Delsing
Department of Microelectronics and Nanoscience, MC2, Chalmers University of Technology and Göteborg University, S-41296 Gothenburg, Sweden

K. W. Lehnert,[b] Lafe Spietz, and R. J. Schoelkopf
Department of Applied Physics and Physics, Yale University, New Haven, Connecticut 06520-8284

(Received 5 September 2003; accepted 29 October 2003)

We have analyzed a radio-frequency single-electron-transistor (RF-SET) circuit that includes a high-electron-mobility-transistor (HEMT) amplifier, coupled to the single-electron-transistor (SET) via an impedance transformer. We consider how power is transferred between different components of the circuit, model noise components, and analyze the operating conditions of practical importance. The results are compared with experimental data on SETs. Good agreement is obtained between our noise model and the experimental results. Our analysis shows, also, that the biggest improvement to the present RF-SETs will be achieved by increasing the charging energy and by lowering the HEMT amplifier noise contribution. © *2004 American Institute of Physics.*
[DOI: 10.1063/1.1635972]

I. INTRODUCTION

The radio-frequency single-electron transistor (RF-SET)[1] is the fastest and most sensitive electrometer known today. Many schemes proposed for sensitive measurement applications have invoked the promise of the RF-SET for fast and ultrasensitive charge detection. These include quantum bits based on nuclear spins in silicon,[2] charged particle detectors,[3] quantum nanomechanical oscillations,[4] and single terahertz photon counters.[5–8] It is one of the only tools for detecting single electron charges at the nanometer scale and with gigahertz bandwidth. Although the RF-SET has approached, but not yet achieved, quantum-limited sensitivity,[9] this does not represent a fundamental limit of the RF-SET as a detector. A combination of practical factors have limited the ultimate sensitivity of the RF-SET.

In this article, we take an electrical engineering approach to the RF-SET system: it is treated as two cascaded amplifiers, as illustrated in Fig. 1(a). Ideally, the shot noise of the first amplifier [single-electron transistor (SET)] dominates the cascade noise properties. However, in the present day RF-SET systems, the second amplifier [high-electron-mobility transistor (HEMT)] sets the noise floor. The scope of this article is to present estimates for the charge and energy sensitivities of practical RF-SET devices by taking into account the noise of the second stage HEMT amplifier accurately. A general conclusion of our noise analysis is that, even in the case of the best matching, the commonly used state-of-the-art cryogenic HEMT amplifiers limit the overall sensitivity. In order to take full advantage of the low noise power of a SET, the HEMT amplifier should be replaced by a low-noise, high-frequency superconducting-quantum-interference-device (SQUID) amplifier,[10] reaching a noise temperature of 200 mK or below.

The article is organized as follows: in Sec. II, the RF-SET system under consideration is defined and an equivalent model is presented. Signal detection is modeled and analyzed in Sec. III, and an estimate for the signal-to-noise ratio is given. Section IV discusses the shot noise of a SET in the noise power wave formalism. The experimental setup is explained in Sec. V, which also shows how the model parameters for the impedance matching circuitry and the amplifier noise characteristics are extracted from the measurements. The modeled signal-to-noise ratio, i.e., the calculated charge sensitivity, is compared with the experimental values, both for Al and carbon nanotube SETs. Finally, Sec. VI explains in detail how charge and energy sensitivities are changed as circuit parameters of a RF-SET setup vary.

Since this article is intended to be a practical guide for a physicist considering the use of a RF-SET in their measurements, we have included many appendices that give specific engineering expressions. This article discusses a more extended analysis on the RF-SET than examined previously in Ref. 11. In Appendix A, explicit expressions for matching circuits in the *S*-parameter formalism are given. Appendix B elaborates in detail how power is transferred between different components of the system. Appendix C gives a short introduction to different noise parameter formalisms. Emphasis is on the noise power wave formalism that is used to extract amplifier noise parameters. In Appendix D, transformation to the common Rothe–Dahlke noise parameter model is given.

II. RF-SET

A metallic single electron transistor is essentially formed by a small piece of metallic conductor, called an island, that

[a]Electronic address: leif.roschier@hut.fi
[b]Permanent address: JILA, National Institute of Standards and Technology and University of Colorado, Boulder, CO 80309.

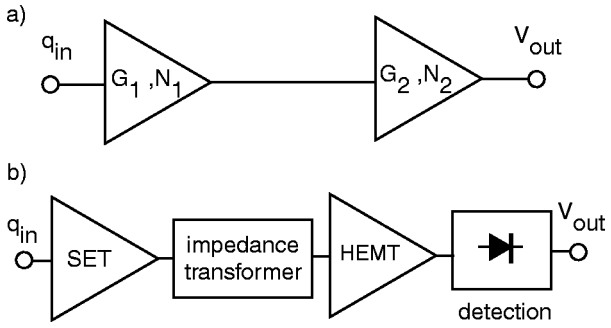

FIG. 1. (a) RF-SET system viewed as a combination of two amplifiers. The first amplifier is a SET with a gain $G_1=\partial P_{\text{out}}/\partial q$ and a charge noise $N_1=\delta q$, where q and P denote charge and power, respectively. The second stage is a power amplifier with $G_2=\partial V_{\text{out}}/\partial P_{\text{in}}$ and noise N_2. (b) A more detailed block diagram of the measurement system. The charge q_{in} is first converted into a power using the SET, then transformed into a wave with 50 Ω impedance and amplified. Finally, the power is converted into a signal voltage using detection circuitry.

is coupled to two electrodes via tunnel junctions.[12] The discreteness of charge and the small total capacitance of the island cause the current to be a periodic function of the gate charge with a period of one electron charge, e. Due to this periodic modulation, a SET may be used as an electrometer with subelectron sensitivity.

In low-frequency operation, the charge sensitivity of a SET is limited by $1/f$ noise, which is, typically, $\geqslant 3\times10^{-4}e/\sqrt{\text{Hz}}$ at 10 Hz for metallic SETs.[13] The bandwidth of a direct readout is limited to approximately 10^5 Hz by the high resistance $\sim 50-200$ kΩ of the SET and the large capacitance ~ 0.1 nF shunting its output. The bandwidth has been increased to 1 MHz by using a low-temperature amplifier close to the SET.[14,15] Such an approach has, however, serious problems due to the power dissipation of the amplifier that increases the sample temperature.

The major advantages of a RF-SET, compared with a direct readout device, are broad bandwidth (up to 100 MHz) and high charge sensitivity.[16] This means that data can be collected orders of magnitude faster than with a direct readout.

The basic principle of a RF-SET is that a carrier wave, usually in the frequency range of 0.1–2 GHz, is reflected from a combination of an impedance transformer circuit and a SET, as illustrated in Fig. 2. The impedance transformer transforms the high impedance of the SET close to 50 Ω, the impedance of a regular transmission line. The change in charge δq at the gate changes the SET impedance R_{SET}, and thus the dissipated power of the carrier wave. The signal δq is carried as amplitude modulation in the reflected wave. A SET is a nonlinear device, in general, but in this article we approximate it as a linear, real impedance controlled by the gate charge. We thus assume that there is only a small amount of mixing from carrier frequency to its harmonics. To take the impedance as real provides a good approximation as long as the capacitance across the SET ($\leqslant 1$ fF) is much smaller than the shunting capacitance C ($\geqslant 100$ fF) of the impedance transformer (see Fig. 2).

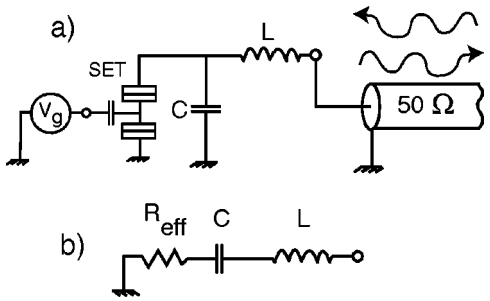

FIG. 2. (a) Model for SET and resonant circuit. (b) Series approximation for the circuit.

Another possibility to implement RF-SET is a transmission configuration, where the transmission amplitude of the rf wave is modulated depending of the SET impedance.[17] In this configuration, one does not need a directional coupler to separate incoming and outgoing waves, as is the case in the reflection configuration.

The circuit describing the SET and the matching circuit in Fig. 2(a) have an impedance

$$Z=j\omega L+\frac{R_{\text{SET}}}{j\omega CR_{\text{SET}}+1}. \tag{1}$$

This impedance may be approximated as a series LCR resonant circuit near the resonance frequency $f_{\text{res}}=1/(2\pi\sqrt{LC})$ when $\omega CR_{\text{SET}}\gg 1$, as illustrated in Fig. 2(b), with the impedance

$$Z=R_{\text{eff}}+j\omega L+\frac{1}{j\omega C}, \tag{2}$$

where

$$R_{\text{eff}}=\frac{L}{CR_{\text{SET}}}. \tag{3}$$

The LC circuit works the same way as a λ/4 transmission line transformer[18] with characteristic impedance $\sqrt{L/C}$. The frequency response of the series resonant circuit in Fig. 2(b) close to the resonance is

$$Z=R_{\text{eff}}+j\frac{2\sqrt{\frac{L}{C}}\Delta\omega}{\omega_0}. \tag{4}$$

The reflected amplitude of the rf wave is expressed with complex reflection coefficient Γ. The relation between Z and Γ is

$$\Gamma=\frac{Z-Z_0}{Z+Z_0}, \tag{5}$$

where Z_0 is the characteristic impedance of a transmission line.

By looking at the Smith chart representation[18] of Γ (Fig. 3), one can visualize how R_{SET} changes the reflected wave. Γ at the LC resonance ($Z=R_{\text{eff}}$) is represented as a point on the real axis (x axis) in the Smith chart. Increasing R_{SET} moves this point to the left. The circles in Fig. 3 illustrate the ideal frequency response described by Eqs. (4) and (5). Appendix A defines a more general formalism expressing $\Gamma(R_{\text{SET}})$ by S matrices. In the S-matrix formalism it is easier to describe more realistic resonator circuits including the

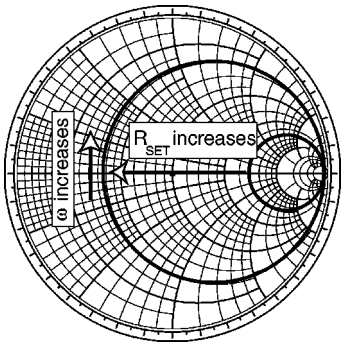

FIG. 3. Smith chart representation of an ideal resonance. Large and small solid circles correspond to an overcritically and undercritically coupled resonator, respectively.

parasitic terms of available passive components. If $R_{\text{eff}} < Z_0$, the SET is overcoupled, and if $R_{\text{eff}} > Z_0$, the SET is undercoupled to the feedline. The coupling is a measure of which component limits the LC resonance bandwidth. In the undercoupled case, the SET and the LC circuit limit the system resonance bandwidth, while the external generator impedance Z_0 is the limiting factor in the overcoupled case. We may define unloaded quality factor $Q_{\text{SET}} = R_{\text{SET}}/\sqrt{L/C}$ and external quality factor $Q_e = \sqrt{L/C}/Z_0$. The total (loaded) quality factor Q_L that sets the bandwidth is then $1/Q_L = 1/Q_{\text{SET}} + 1/Q_e$.

III. SIGNAL-TO-NOISE RATIO AFTER DETECTION

We start the analysis for the signal-to-noise ratio by defining a model for the reflected signal amplitude from the impedance transformer:

$$v_0[\Gamma_0 + \Delta\Gamma \cos(\omega_m t)]\cos(\omega_0 t) + n(t), \tag{6}$$

where the reflection coefficient Γ is modulated sinusoidally with $\Delta\Gamma \cos(\omega_m t)$ at the working point Γ_0. ω_m is the modulation frequency, ω_0 is the carrier frequency ($\omega_m \ll \omega_0$), and v_0 the amplitude of the incoming voltage wave. $n(t)$ is the noise term in the time domain. If $\Gamma_0 \neq 0$, the scheme corresponds to the *amplitude modulation* (AM).

We assume that the signal (and noise) has been amplified sufficiently, so that the noise added by the detection is negligible. The signal and carrier components from Eq. (6) can be written in the form

$$s \equiv v_0\Gamma_0 \left\{ \cos(\omega_0 t) + \frac{\Delta\Gamma}{2\Gamma_0}\{\cos[(\omega_0 - \omega_m)t] + \cos[(\omega_0 + \omega_m)t]\} \right\}. \tag{7}$$

The power spectrum consists of the carrier component at frequency ω_0 and two side peaks at a distance $\pm\omega_m$ from the carrier. In the following analysis we assume that $\Delta\Gamma/\Gamma_0 \ll 1$ for diode detection (signal squared), since otherwise there will be contributions from sideband modulated noise. Also, if $\Gamma_0 \sim 0$, the approximation that the carrier $\cos(w_0 t)$ multiplies the signal turns out incorrect. In other words, we assume that the carrier amplitude exceeds the side-peak amplitudes substantially in diode detection. For homodyne detection [signal multiplied with $\cos(w_0 t)$], there is no such constraint for the validity of the analysis below, since there is no need for a dominant carrier signal to multiply side-peak signals.

After detection the signal component d is

$$d \equiv s\cos(\omega_0 t) = v_0 \frac{\Delta\Gamma}{2}\cos(\omega_m t). \tag{8}$$

This signal has a root-mean-square (rms) amplitude

$$\sqrt{S_d} = v_0 \frac{\Delta\Gamma}{\sqrt{8}}. \tag{9}$$

The noise component $n(t)$ (assumed to have a white spectrum) is characterized by an equivalent temperature T_0, such that

$$S_V = k_B T_0 Z_0, \tag{10}$$

where $Z_0 \sim 50\ \Omega$ is the characteristic impedance of the rf lines and the first-stage-amplifier input impedance. S_V is the power spectral density of voltage fluctuations over the amplifier input impedance. The equivalent temperature T_0 includes all noise sources affecting the SET readout. It is to be noted that T_0 is not the effective extended noise temperature T_{ee} that is defined by a voltage noise generator with spectral density $S_V = 4k_B T_{ee}\,\text{Re}(Z_S)$ in series with the source impedance Z_S.[19]

In order to compare signal and noise after detection, one has to calculate the power spectral density S_y of the noise after detection

$$y(t) \equiv n(t)\cos(\omega_0 t), \tag{11}$$

which yields[20]

$$S_y(\omega) = \tfrac{1}{4}[S_V(\omega - \omega_0) + S_V(\omega + \omega_0)]. \tag{12}$$

When both negative and positive frequency parts of the term $S_V(\omega - \omega_0)$ are taken into account (we return to think in terms of only positive frequencies), we find for the rms noise amplitude per unit band

$$\sqrt{S_y} = \sqrt{\frac{k_B T_0 Z_0}{2}}. \tag{13}$$

The signal-to-noise (S/N) ratio becomes

$$\frac{S}{N} = \sqrt{\frac{S_d}{S_y}} = \frac{v_0\Delta\Gamma}{\sqrt{4k_B T_0 Z_0}}. \tag{14}$$

This can be converted into an effective charge noise expressed in units of $e/\sqrt{\text{Hz}}$ using the equation:

$$\Delta\Gamma = \sqrt{2}\Delta\Gamma_{\text{rms}} = \frac{\partial\Gamma}{\partial q}\sqrt{2}\,\delta q_{\text{rms}}, \tag{15}$$

where rms quantities are used because the charge noise is, typically, measured in terms of rms values. By setting S/N $= 1$ in Eq. (14), we find

$$\delta q_{\text{rms}} = \frac{\sqrt{2k_B T_0 Z_0}}{v_0 \dfrac{\partial|\Gamma|}{\partial q}}. \tag{16}$$

This is the basic equation for the charge resolution of a RF-SET having readout circuitry with an equivalent noise temperature of T_0.

A. Estimated optimum performance for RF-SET

The most sensitive RF-SET system can be realized by minimizing Eq. (16). First, the term in the denominator v_0, the voltage amplitude of the incoming wave, has to be converted to a voltage over the SET. This can be done using the power coupling coefficient K (defined formally in Appendix B). The quantity K is the proportion of the available power that is coupled to the SET from a voltage generator with series impedance Z_0. The available power of an incoming wave is $v_0^2/2Z_0$, and a fraction K of this power is coupled to the SET. An equivalent expression for the dissipated power is given by $v_{\mathrm{SET}}^2/2R_{\mathrm{SET}}$, where v_{SET} is the amplitude of ac voltage across the SET. Thus, one obtains the relation

$$v_0 = v_{\mathrm{SET}} \sqrt{\frac{Z_0}{R_{\mathrm{SET}} K}}, \tag{17}$$

between v_0 and v_{SET}. The charge sensitivity in Eq. (16) now takes the form

$$\delta q = \frac{\sqrt{2 k_B T_0 R_{\mathrm{SET}} K}}{v_{\mathrm{SET}} \dfrac{\partial |\Gamma|}{\partial q}}. \tag{18}$$

In general, the optimization of Eq. (18) will include many details of the SET's behavior, and can be quite complicated. For example, the analysis here has assumed that the SET behaves as a linear impedance, which depends only on the gate charge. In order to maximize the sensitivity, the rf voltage on the drain and source of the SET, v_{SET}, should be made as large as possible. However, it is clear that a large amplitude for v_{SET} will eventually probe the nonlinearity of the SET's conductance, or that the effective reflection coefficient will cease to depend on the gate. The maximum allowable value of v_{SET}, and of the product $v_{\mathrm{SET}}(\partial|\Gamma|/\partial q)$, will therefore depend on the dc drain–source bias, whether the SET is normal or superconducting, the temperature of operation, and many other variables. As a first step, in this article we treat the simplest case, a normal SET with zero drain–source bias. By examining the current–voltage of a normal SET (see, e.g., Fig. 5), we see that the maximum change in resistance of the SET occurs at zero bias, and that the gate modulation extends only to a maximum voltage of order the Coulomb blockade threshold voltage, E_C/e, where $E_C = e^2/2C_\Sigma$ and is governed by the total island capacitance C_Σ. If all the other parameters (including the resistance of the SET) can be held fixed, a higher charging energy allows a larger maximum voltage, and in turn a lower charge noise contribution from the readout amplifier. This type of reasoning also assumes that the SET's response to the rf voltage is instantaneous, or that the tunneling rate through the device is larger than the frequency of the rf excitation. Although Eq. (18) requires simplified or phenomenologically determined values of the optimum voltage and the gate modulation of the impedance $(\partial|\Gamma|/\partial q)$, with these inputs it allows the charge sensitivity to be simply expressed in terms of practical parameters, and can then be used in minimizing the noise added by the rf readout of the SET.

IV. DEPENDENCE OF SYSTEM NOISE TEMPERATURE ON SET IMPEDANCE AND BIAS

The preceding sensitivity analysis ignores both the low-frequency $1/f$ noise, and the intrinsic (shot) noise of the SET, and furthermore, assumes that the system noise temperature is independent of the impedance at the rf amplifier's input, which can in fact vary as the SET's impedance varies with gate. In this section, we present a more complete model for the system noise, which allows us (cf. Sec. V C) to use the dependence on the drain–source and gate bias of the SET to extract the full noise properties of the rf amplifier. First, we assume that an amplifier (power gain G_P) with correlated noise wave amplitudes A_n moving towards amplifier input and B_n moving towards the SET (see Appendix C), we can write down a formula for the noise power N_P over the bandwidth B

$$N_P = G_P B(\overline{|A_n|^2} + |\Gamma|^2 \overline{|B_n|^2} + 2\,\mathrm{Re}(\Gamma \overline{A_n^* B_n}) + \mathrm{N} k_B T_m). \tag{19}$$

In Eq. (19) Γ is the reflection coefficient of the noise wave from the SET and resonant circuit [Fig. 2(a)]. The quantity N (defined formally in appendix B) is the fraction of the available power dissipated in the resonant circuit.

System noise can also have a contribution from the shot noise of the drain–source current through the SET, which is coupled to the amplifier via the transformer. In the regime of Coulomb blockade ($V_{\mathrm{ds}} \leqslant E_c/e$), this shot noise has a complex dependence on the drain and gate bias, and a Fano factor which depends on correlations in the tunneling through the two junctions. However, in the practical case we consider, where the HEMT amplifier is dominant, the shot noise contribution is small except at large drain–source bias. At high bias, we can treat the SET as a series array of two uncorrelated tunnel junctions, each of which has a spectra density given by the formula[21]

$$S_I = \frac{2eV_J}{R_{\mathrm{jct}}} \coth \frac{eV_J}{2k_B T}. \tag{20}$$

If the junctions are identical, we have to multiply Eq. (20) with a Fano factor of 0.5 if the tunneling processes between the two junctions are uncorrelated. Also, for the resistance we have to use the total resistance R_{tot} over both junctions. In this case, we find for the power spectral density

$$S_P = S_I R_{\mathrm{tot}} = eV \coth \frac{eV}{4k_B T}, \tag{21}$$

where $V = 2V_J$ is the total voltage across the two junctions. The maximum power that can be delivered from the SET to a load impedance (i.e., amplifier input impedance) is the available power $S_P/4$. This maximum power transfer occurs when the source and load impedances are conjugate matched ($Z_{\mathrm{SET}} = Z_{\mathrm{load}}^*$). We can then rewrite Eq. (19), now including the shot noise contribution, in a form suitable for fitting:

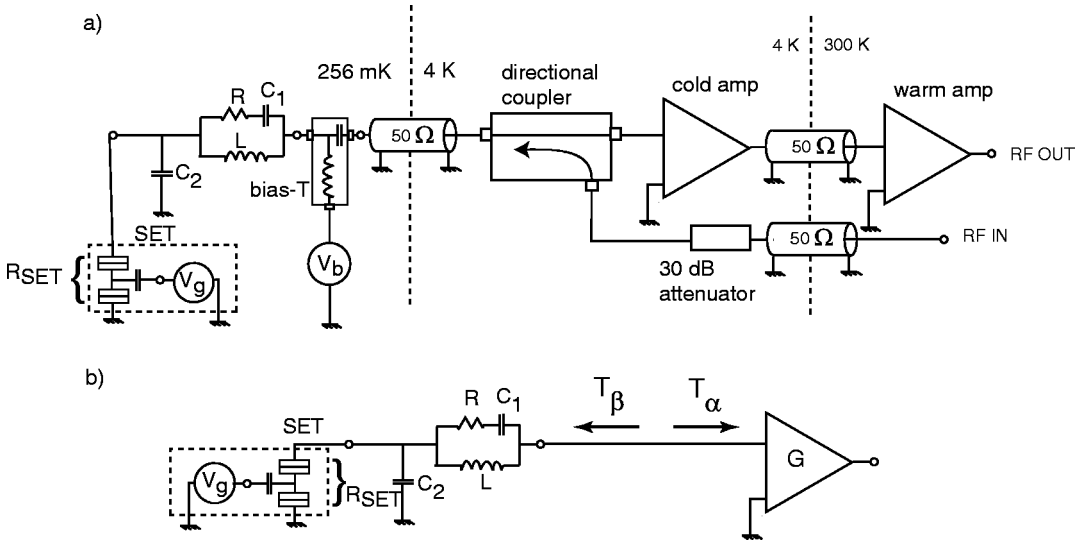

FIG. 4. Measurement setup. (a) A carrier wave is guided down to the SET using the RF IN line. An attenuator of 30 dB and a directional coupler with 13 dB loss attenuate thermal noise. The wave is reflected from the SET with an LC matching circuit and amplified with a chain of cold and warm amplifiers. The signal is detected from RF OUT port using a diode detector. (b) Noise measurement schematic. The amplifier incorporates all the components starting from bias-T to the warm amplifier. T_α and T_β illustrate two correlated noise power waves at the amplifier input. Noise measurement bandwidth was 5 MHz.

$$N_P = G_P B\Big(k_B T_\alpha + |\Gamma|^2 k_B T_\beta - 2|\Gamma| k_B T_\gamma \cos(\phi_\gamma + \phi_s) + \mathrm{N} k_B T_m + \mathrm{K}\frac{eV}{4}\coth\frac{eV}{4k_B T}\Big), \tag{22}$$

where the T noise parameters, defined in Ref. 19,

$$\overline{|A_n|^2} = k_B T_\alpha, \quad \overline{|B_n|^2} = k_B T_\beta, \quad \overline{A_n^* B_n} = -k_B T_\gamma e^{j\phi_\gamma}, \quad \Gamma = |\Gamma| e^{j\phi_s}, \tag{23}$$

are employed. In practice, this noise power N_P divided by $(G_P B k_B)$ yields the equivalent noise temperature T_0 that determines the SET sensitivity according to Eq. (16). In the format of Eq. (22), T_0 depends on source reflection coefficient Γ. In our SET sensitivity analysis, we assume T_0 to be a constant for simplicity. As seen in Sec. V C, this assumption turns out to be valid experimentally.

V. EXPERIMENTAL RESULTS

In order to test the formalism described in the previous sections, we have measured the properties of two SETs: one $Al/AlO_x/Al$ device and one carbon nanotube SET. We will discuss mostly the results on the Al SET and use these results, also, to characterize the measurement system thoroughly. Our measurements were done in a ^{3}He refrigerator at $T = 256$ mK. The scheme of the electronic measurement setup is illustrated in Fig. 4(a). The effective circuit of the noise measurements is illustrated in Fig. 4(b). In the noise analysis the directional coupler, the stainless steel coaxial cable, the bias-T, and the second stage amplifiers had to be treated as a single amplifier unit. In the noise modeling, the effective noise of this amplifier unit deviates from the cryogenic HEMT amplifier[22] alone, mostly due to the electrical delay and attenuation of the directional coupler, the stainless steel coaxial cable (probably the biggest effect), and the bias-T. The dc lines to bias the SET and the gate were filtered with stainless steel powder filters.[23]

A. Extraction of matching network parameters

Figure 5 illustrates the measured current–voltage characteristics, together with numerically derived conductance curves from them. The inverse of the conductance was taken as the resistance of the SET; the reactance of the SET was assumed to be zero. Using ''orthodox theory,''[24] the measured IV curve at maximum blockade can be reproduced accurately with the parameters: $E_C/k_B \sim 1.13$ K, $T = 280$ mK, and a total large-bias resistance of $R_\Sigma = 46\ \mathrm{k}\Omega$.

Figures 6 and 7 illustrate the measured frequency response of the zero-bias SET. The resonance dip due to the LC matching circuit is clearly visible (at 471.2 MHz). The data were extracted by measuring S_{21} between ports rf IN and rf OUT in Fig. 4 with a network analyzer. This corresponds to a measurement of the reflection coefficient Γ. The measured S_{21} included the influence of unknown attenuation and electrical delay from the components between the rf generator and the resonant circuit [Fig. 4(a)]. In order to determine Γ, S_{21} was corrected with a single, complex multiplicative factor, determined by fitting the observed dependence of S_{21} vs ω and S_{21} vs R_{SET} to a detailed S-parameter model (Appendix A) of the resonant circuit (Figs. 7 and 8).

The corrected Γ is illustrated in Fig. 6, along with an ideal resonance circle. Extra ripples in the frequency response are probably due to some amplifier and input cable resonances. Also, slight gain variation with frequency is visible. These deviations from the ideal situation made the correction procedure discussed above a formidable task. It is to be noted that the dip in $|\Gamma|$ is deep for both the maximum and minimum blockades in Fig. 7. This is due to the lossy impedance transformer that was implemented using a surface-mount inductor formed from copper wire wound on a ce-

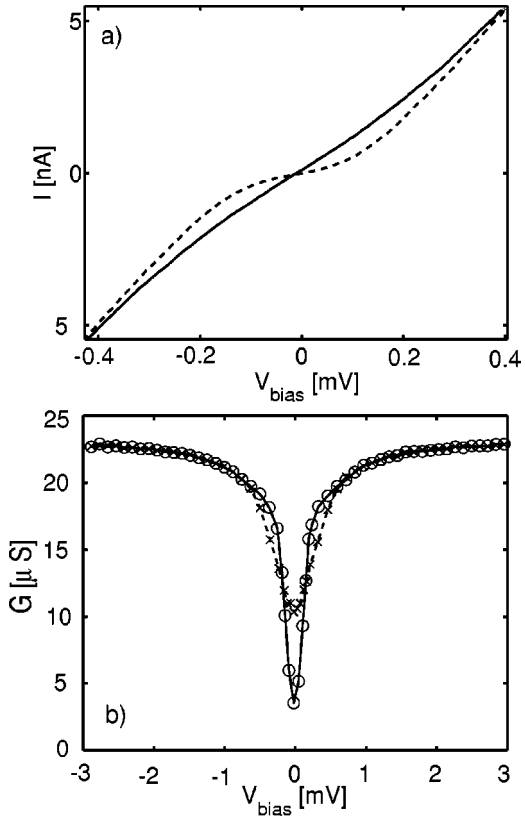

FIG. 5. (a) *IV* curves measured at maximum (dashed) and minimum (solid) Coulomb blockade. (b) Numerically calculated conductance from the measured *IV* curves in (a). The two curves correspond to the cases of maximum (○) and minimum (×) Coulomb blockade.

ramic core and a capacitor formed from the stray capacitance to ground between the inductor and the SET [Fig. 2(a)].

After the resonance frequency $f_0 = 471.2$ MHz was found by measuring the frequency response with a network analyzer, we measured $|\Gamma|$ as a function of the bias and gate voltages. Diode detection was used to measure the reflected power [Fig. 1(b)]. The result is illustrated in Fig. 8. It is apparent that the LC-matched SET is undercritically coupled at zero bias (R_{SET} high) and passes through critical to overcritical coupling (R_{SET} small) as the bias voltage is increased (Sec. II). This behavior made the fitting more accurate because $|\Gamma|$ passed via zero, i.e., through the center of the Smith chart.

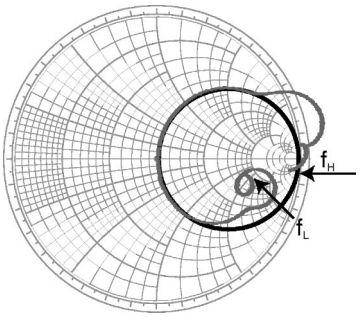

FIG. 6. Smith chart representation of the measured, corrected reflection coefficient (Γ) along with an ideal resonance circle. The lower and upper ends of the frequency sweep are denoted by f_L and f_H.

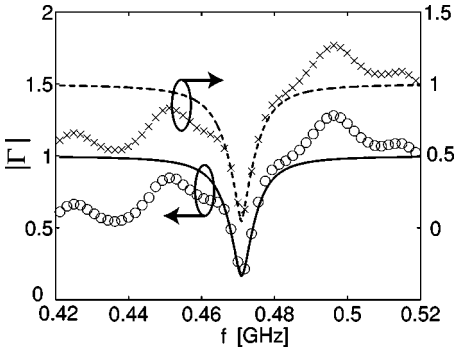

FIG. 7. $|\Gamma|$ at zero bias vs frequency measured for the Al SET at gate charge values corresponding to the minimum (×) and maximum (○) Coulomb blockade state. Solid and dashed curves are fits using the lumped-element impedance transformer and the measured zero-bias resistances $R_{\mathrm{SET}}^{\mathrm{min}}$ and $R_{\mathrm{SET}}^{\mathrm{max}}$, respectively. The curves at minimum Coulomb blockade are shifted upwards by 0.5 units to enhance visibility.

We employed the S-matrix representation defined in Appendix A to extract parameters C_1, C_2, R, and L from the reflection measurements done over the whole variable range of R_{SET}. The extracted parameters are tabulated in Table I. The curves obtained using these parameters at both the maximum and minimum Coulomb blockade are displayed in Figs. 7 and 8. As seen in Fig. 8, the bias dependence of the reflection coefficient $\Gamma(V_{\mathrm{bias}})$ is very well reproduced with the matching circuit parameters of Table I; the agreement in the frequency dependence is spoiled by the unknown resonances as mentioned before.

The calculated values of K, N, and $|\Gamma|$ are illustrated in Fig. 9 as a function of R_{SET}. It is interesting to notice that K and N have slopes of opposite signs when $R_{\mathrm{SET}} > 40\ \mathrm{k}\Omega$. This degrades the RF-SET performance because $\partial|\Gamma|/\partial R_{\mathrm{SET}}$ becomes smaller.

B. Calculated versus measured charge noise

From the slope of the measured transfer function illustrated in Fig. 10, we can estimate the variation of R_{SET} with respect to the gate charge

$$\frac{\partial R_{\mathrm{SET}}}{\partial q} = 3.44 \Delta R \frac{1}{e}, \tag{24}$$

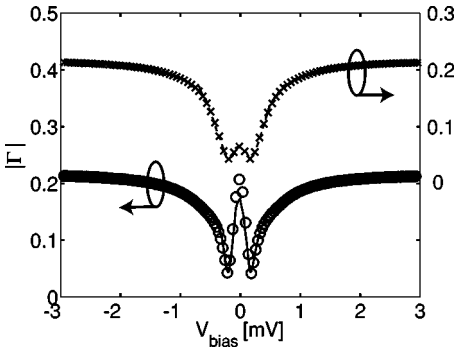

FIG. 8. Measured (symbols) and calculated (dashed and solid lines) values of $|\Gamma|$ vs bias voltage at maximum (○) and minimum (×) Coulomb blockade. The minimum blockade curve is shifted 0.2 units upwards to increase visibility.

TABLE I. Parameters extracted from reflection measurements for the impedance transformer.

C_1 (pF)	C_2 (pF)	R (Ω)	L (nH)
0.239	0.208	12.0	256

where ΔR is the maximum change in resistance that the gate can induce. For our Al sample $\Delta R = 44.5\ \mathrm{k}\Omega$, which yields $\partial R_{\mathrm{SET}}/\partial q = 153\ \mathrm{k}\Omega/e$. We take $v_{\mathrm{SET}} = E_c/e = 156\ \mu\mathrm{V}$ for the optimum ac amplitude over the SET; this is the maximum voltage at which the resistance swing ΔR still remains at its largest value. By using the fitted parameters of the lumped-element matching circuit in the S-matrix formulation, we obtain $\partial|\Gamma|/\partial R_{\mathrm{SET}} = 2.6\ \mu\mathrm{S}$ from Eq. (5) at the approximate operating point with $R_{\mathrm{SET}} = 111.7\ \mathrm{k}\Omega$, which corresponds to the position of highest slope on the transfer function in Fig. 10. For K we calculate a value of 0.62. Then, by using Eq. (18) and a constant value of $T_0 = 4\ \mathrm{K}$, as is suggested by Fig. 11, we find that the charge sensitivity becomes $4.4\times10^{-5} e/\sqrt{\mathrm{Hz}}$.

For reference, we calculated IV curves as a function of gate charge using orthodox theory with parameters $T = 280\ \mathrm{mK}$, $R_\Sigma = 46\ \mathrm{k}\Omega$, and $E_C/k_B = 1.13\ \mathrm{K}$. From the calculated IV curves we determined an effective rms resistance $R_{\mathrm{rms}} \equiv \sqrt{\langle U^2\rangle/\langle I^2\rangle}$ as a function of the ac voltage amplitude over the SET. U and I are the instantaneous voltage and current of the SET, respectively. The average $\langle\cdots\rangle$ is taken over one complete ac period. Then, by numerical minimization of Eq. (18), we found the ac voltage amplitude and gate charge for the best charge sensitivity. At the optimum operating point, we obtained $R_{\mathrm{rms}} = 124\ \mathrm{k}\Omega$, $v_{\mathrm{SET}} = 152\ \mu\mathrm{V}$, and a charge sensitivity $\delta q = 3.5\times10^{-5} e/\sqrt{\mathrm{Hz}}$.

These theoretical values can be compared with the charge noise measured at frequency 1.1 MHz, where the contribution from the low-frequency $1/f$ charge noise is negligible. At $V_{\mathrm{bias}} = 0$, we measured $\delta q = 3.8\times10^{-5} e/\sqrt{\mathrm{Hz}}$ using optimized ac amplitude and gate voltage. The first theoretical estimation using the transfer function gave a less accurate estimate, owing to a large uncertainty in the values of v_{SET} and $\partial R_{\mathrm{SET}}/\partial q$. In the latter estimation, using the calculated IV curves, the result agreed with measurements within $\pm 10\%$. Thus, our model, taking into account the amplifier noise and the relevant passive components with fitted parameter values, explains the measured charge sensitivity.

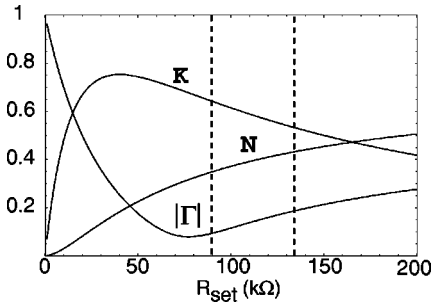

FIG. 9. The fraction of available power coupled to the load (K) and to the coupling network (N), as well as the reflection coefficient $|\Gamma|$. For our Al-SET, the dashed lines limit the range of R_{SET} that is usable for finding the optimum operating conditions.

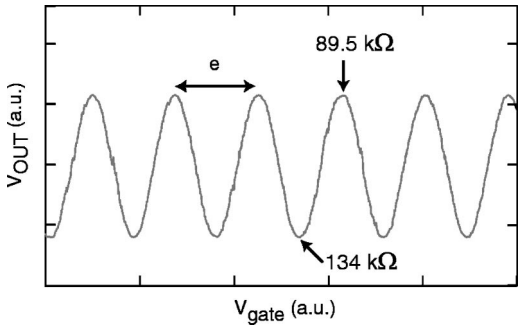

FIG. 10. Measured transfer function, i.e., output voltage from detection vs gate voltage. One period corresponds to a change of charge by e on the island. The minimum and maximum values of V_{OUT} correspond to $R_{\mathrm{SET}} = 134$ and 89.5 kΩ, respectively.

The charge noise of the aluminum RF-SET is mostly dominated by the amplifier noise in our measurement system. In our analysis of the charge sensitivity, in fact, we have included only the noise from the amplifier system. The intrinsic shot-noise limit of a RF-SET is expected to be $1.4\times10^{-6} e/\sqrt{\mathrm{Hz}}$,[25] so it is safe to neglect the shot-noise contribution in the present analysis.

Our aluminum RF-SET has an uncoupled energy sensitivity of $\delta q^2/2C_\Sigma \sim 340\hbar$. If the lossy impedance transformer were changed to an ideal lossless one, then this sensitivity would become $\sim 220\hbar$.

C. Shot-noise calibration of amplifier noise

In order to characterize the noise properties of the amplifier setup after the tank circuit, we fitted Eq. (22) to the noise measured as a function of current. In other words, we used the shot-noise of Eq. (21) as a calibration standard. The four extracted parameters in the noise power wave formalism are tabulated in Table II. The fitted curves and the measured data are depicted in Fig. 11. It is obvious that the amplifier

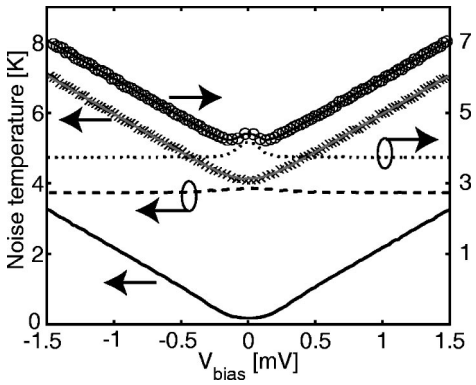

FIG. 11. Measured noise power NP/($k_B BG$) in Kelvins at minimum ($\times$) and maximum ($\bigcirc$) Coulomb blockade. The two topmost solid lines correspond to the fits obtained from Eq. (19) using the parameters of Table II. The dashed and dotted lines are amplifier contributions to the measured noise for maximum and minimum Coulomb blockade, respectively. The lowest solid curve illustrates the shot noise contribution to the measured noise.

TABLE II. Extracted noise parameters in the power wave formalism for the amplifier setup including the components from the impedance transformer output up to the last warm amplifier output (see Fig. 4). For definitions of the parameters, see Appendix C and Eq. (23).

T_α (K)	T_β (K)	T_γ (K)	ϕ_γ (rad)
3.78	1.22	0.35	0.56

adds a noise power corresponding to ~ 4 K to the input signal over the whole bias range. Thus, our assumption of constant amplifier noise is quite well justified.

Figure 12 illustrates the effect of a varying reflection coeffiecient Γ on the amplifier noise. As the noise matching changes, the effective noise temperature varies between ~ 3.7 and 5 K. Perfect power matching with $|\Gamma|=0$ is seen to be rather close to the optimum noise matching in our setup.

VI. MINIMIZATION AND SCALING OF THE CHARGE NOISE ADDED BY THE RF READOUT

In the previous section we showed that our model for calculating charge sensitivities of SETs agrees well with the measured, experimental values. In this section, we use the same model, i.e., Eq. (18), to estimate how good a charge resolution can be achieved with a given set of parameters, keeping them still within the realm of technological feasibility.

The term $\partial|\Gamma|/\partial q$ is computed using $I(V_{\mathrm{SET}}, q_{\mathrm{gate}}, t, T_{\mathrm{EC}}, R_\Sigma)$ surfaces calculated with orthodox theory; $t = k_B T/E_C$ is the normalized temperature and T_{EC} is the charging energy E_C in kelvins. As an effective resistance of the SET we use $R_{\mathrm{rms}}=\sqrt{\langle U^2\rangle/\langle I^2\rangle}$, where the average $\langle\cdots\rangle$ is taken over one complete ac period. For matching, we use an ideal lossless LC-resonator impedance transformer as described in Sec. II. The impedance transformer is characterized by an impedance $Z_T \equiv \sqrt{L/C}$ alone; no parasitic terms are taken into consideration. Thus, we describe the system with parameters $t, T_{\mathrm{EC}}, R_\Sigma, T_0$, and Z_T. We maximize the charge sensitivity with respect to the variables V_{SET} and q_{gate} under the constraint that the impedance of the matching circuit has $Z_T < 2500\ \Omega$. This impedance constraint is imposed because, when $Z_T \gg 1000$, the Q factors start to limit the measurement bandwidth: $Z_T = 2500\ \Omega$ corresponds to a Q value $\sim 2500\ \Omega/50\ \Omega = 50$, and a bandwidth of 5 MHz if the carrier frequency is 500 MHz. Also, a high-Z_T impedance transformer is more complicated to implement due to the low-frequency self-resonances of a large inductor.

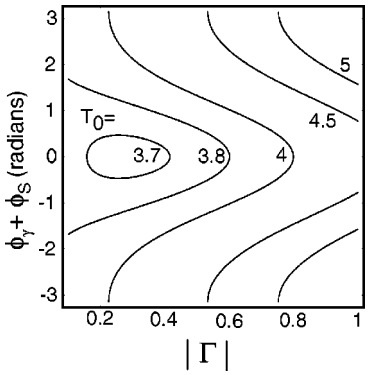

FIG. 12. Amplifier input noise equivalent temperature $T_0 = T_\alpha + |\Gamma|^2 T_\beta - 2|\Gamma| T_\gamma \cos(\phi_S + \phi_\gamma)$ as a function of source reflection coefficient Γ. Note that this is not the usual effective extended noise temperature $T_{ee} = T_0/(1-|\Gamma|^2)$ of the amplifier, where the noise generator is located at the source. For more details, see Appendix D.

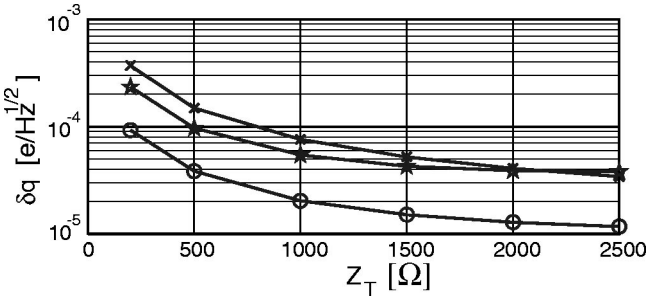

FIG. 13. Charge sensitivity of RF-SET calculated from Eq. (18) assuming an amplifier system with $T_0 = 4$ K. The curves have been obtained with the following parameters: (○) $t = 0.1E_C$, $R_\Sigma = 50$ kΩ, and $E_C = 1$ K; (×) $t = 0.1E_C$, $R_\Sigma = 200$ kΩ, and $E_C = 1$ K; and (★) $t = 0.3E_C$, $R_\Sigma = 50$ kΩ, and $E_C = 1$ K.

Figure 13 illustrates the calculated charge sensitivity as a function of Z_T for an amplifier setup with $T_0 = 4$ K; other contributions to noise have been neglected. Figure 13, and the following ones, can be considered as a set of guidelines for the estimation of technological limitations on charge sensitivity. Some of the employed SET parameters may be difficult to achieve simultaneously: for example, small R_Σ and large T_{EC} are conflicting requirements in aluminum devices. Carbon nanotubes, however, are rather exceptional in this respect and provide a small R_Σ and a large T_{EC} almost routinely, but often at the expense of irregularities in their gate modulation curves. Figure 14 illustrates the charge sensitivity curves assuming an amplifier with $T_0 = 100$ mK. In fact, these curves represent the viable performance of an RF-SET in conjunction with a matched, high-frequency SQUID amplifier.

In order to characterize the unavoidable trade-off between the bandwidth and sensitivity, we plot in Fig. 15 the product of the charge sensitivity and the Q factor of the impedance transformer. This plotted quantity corresponds to the inverse of the gain-bandwidth (GBW) product. Accord-

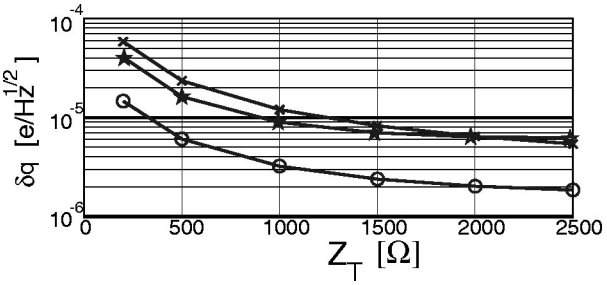

FIG. 14. Charge sensitivity of a RF-SET calculated from Eq. (18) assuming an amplifier system with $T_0 = 100$ mK. The symbols are listed in the caption of Fig. 13.

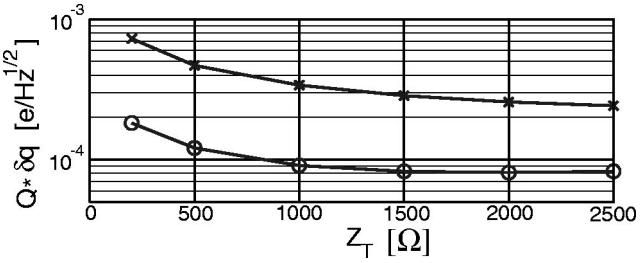

FIG. 15. Charge sensitivity $\times$ Q factor that represents the inverse of gain-bandwidth product. The symbols are listed in the caption of Fig. 13.

ing to Fig. 15, there is not much enhancement in the GBW of the RF-SET once Z_T exceeds 1000 Ω.

The noise added by the readout, expressed as the uncoupled energy sensitivity of a RF-SET, $\epsilon = \delta q^2/2C_\Sigma$ (in units of J/Hz) is shown as a function of the charging energy E_C in Fig. 16. The result depends strongly on the noise temperature of the amplifier. Only when $T_0 = 100$ mK, does the noise approach $\hbar$, on the order of the expected intrinsic noise of the SET.[26] Since our treatment does not include any noise from the SET, one should interpret a predicted energy sensitivity comparable or less than $\hbar$ as a prediction that the noise added in the readout of the SET can be made negligible compared to the SET's noise. In this case, though our analysis does not include the SET noise, we expect that the energy sensitivity of the entire system would approach $\hbar$.

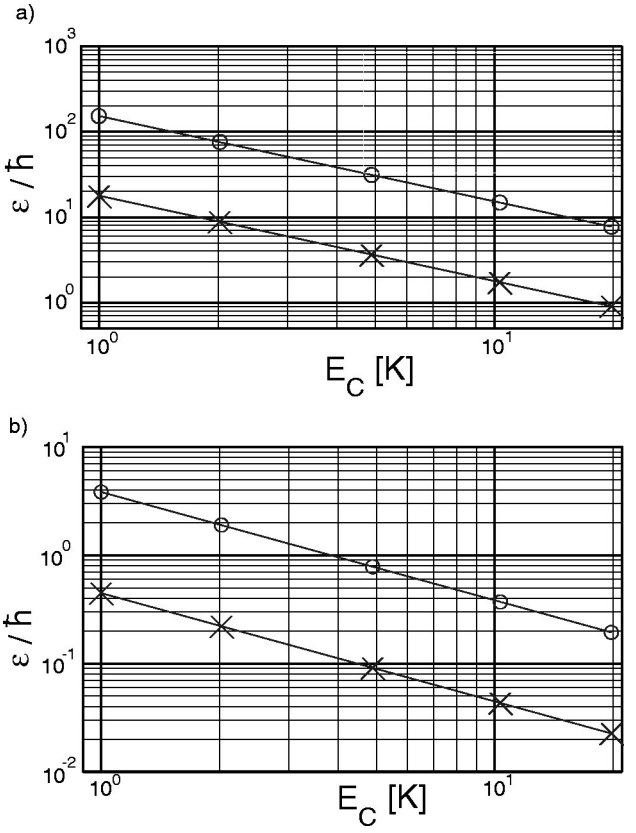

FIG. 16. Contribution of RF readout to the energy sensitivity of a RF-SET. When the predicted contribution to epsilon/hbar approaches 1, the readout's contribution is negligible and the SET's intrinsic limits should be approached. Calculations are for (a) $T_0 = 4$ K and (b) $T_0 = 100$ mK, with an impedance transformer of $Z_T = 2500\ \Omega$. The curves have been calculated with the following parameters: ($\times$) $T = 0.1E_C$ and $R_\Sigma = 50$ kΩ, and ($\bigcirc$) $T = 0.1E_C$ and $R_\Sigma = 200$ kΩ.

All the numerical results above with an ideal impedance transformer can be summarized using a single phenomenological equation for charge sensitivity δq ($e/\sqrt{\text{Hz}}$):

$$\delta q \approx 1.46 \times 10^{-6} Z_T^{-0.91} t^{0.59} T_{\text{EC}}^{-1.01} R_N^{0.91} T_0^{0.5}. \tag{25}$$

The units for the parameters are Z_T (Ω), T_{EC} (K), R_Σ (Ω), and T_0 (K). This formula reproduces the numerical results over $0.01 < t < 0.3$, $200 < Z_T < 2500$, 50 k$\Omega < R_N <$ 200 kΩ with a 50% tolerance.

In order to estimate the SET electron temperature T_{eff} due to the heating from ac bias, we calculate the heating power $P = v_{\text{opt}}^2/(2R_{\text{rms}})$ using the effective resistance $R_{\text{rms}} = \sqrt{\langle U^2 \rangle / \langle I^2 \rangle}$ and the voltage amplitude v_{opt} at each optimum sensitivity point with varying Z_T, T_{EC}, t, R_Σ, and T_0. For the electron temperature we use the model $T \sim [P/(2\Sigma\Omega)]^{1/5}$,[27] where Σ is a constant of order ~ 1 nW/K$^5/\mu$m^3 and Ω is the volume of the SET island that we take to be of order $1 \times 0.2 \times 0.05$ μm^3. By fitting phenomenological formula $aT_{\text{EC}}^{\alpha} R_\Sigma^{\beta}$ to numerical results, we find that formula

$$T_{\text{eff}} \approx 2.45 \times T_{\text{EC}}^{0.4} R_\Sigma^{-0.2}, \tag{26}$$

reproduces simulated results within a 20% tolerance. The units for the parameters are (K) for T_{EC} and (Ω) for R_Σ. We find dissipated power P to be uncorrelated to the parameter $t = T_{\text{eff}}/T_{\text{EC}}$. Equation (26) may be compared with Eq. (32) in Ref. 27 ($T_{\text{eff}} \sim 20 \times E_C^{0.4} R_\Sigma^{-0.4}$), which gives the effective temperature of a SET with dc bias. Both models give similar results when $R_\Sigma \sim 40$ kΩ. One should note that the electron heating is quite considerable and the electron temperature is much greater than the base temperature of the cryogenic apparatus. For example, if $R_\Sigma = 50$ kΩ and $T_{\text{EC}} = 2$ K, the electron temperature due to heating is of order 370 mK. Another conclusion is that in order to reach $t = 0.1$ one needs $T_{\text{EC}} \sim 6$ K.

By combining Eqs. (25) and (26), we get an estimate for the charge sensitivity that takes into account heating effects from ac bias:

$$\delta q \approx 2.48 \times 10^{-6} Z_T^{-0.91} E_{\text{EC}}^{-1.36} R_\Sigma^{0.79} T_0^{0.5}. \tag{27}$$

The units for the formula are (Ω) for Z_T and R_Σ, and (K) for T_{EC} and T_0.

As a test of Eq. (27), we compare the charge sensitivity calculated from it with four measurement results: (1) Al SET in this work above, (2) the original RF-SET,[1] (3) RF-SET at Chalmers,[9] and (4) a device made of a multiwalled carbon nanotube.[28] Table III summarizes the results. The results agree within factor 3.

In Table III, the most poorly known quantity from the measurements is probably Z_T. To calculate Z_T, we have assumed the nominal inductance of the commercial components used in the resonant circuits. Because the resonant frequency of the these circuits is close to the self-resonance frequency of the inductor, the inductor's reactance will significantly exceed Z_T calculated from the nominal inductance. In a more rigorous analysis, Z_T would be determined experi-

TABLE III. Parameters of RF-SET measurements and the estimated charge sensitivity using Eq. (27) except for carbon nanotube sample. In carbon nanotube sample island volume Ω is $\frac{1}{100}$ of the typical metallic SET island volume. This increases the T_{eff} in Eq. (26) by a factor $(\frac{1}{100})^{-1/5}$, which is used in Eq. (25) to calculate δq. The charge sensitivities in Ref. 9 have been taken to be a factor $\sqrt{2}$ better than reported ($9\times10^{-6}e/\sqrt{\mathrm{Hz}}$) due to the fact that in the article sensitivity was calculated from a single sideband. The enhancement comes from the fact that when the signal is mixed down, noise is summed as power, but signal as amplitude. We assume that the first amplifier sets the noise floor and that the spectrum is white.

	This work	Al RF-SET[a]	Al RF-SET[b]	Carbon nanotube RF-SET[c]
Z_T	758 Ω	283 Ω	1293 Ω	900 Ω
T_{EC}	1.13 K	2.1 K	3.5 K	3.5 K
R_Σ	46 kΩ	97 kΩ	43 kΩ	150 kΩ
T_0	4 K	10 K	6.3 K	4 K
δq calculated	$4.8\times10^{-5}e/\sqrt{\mathrm{Hz}}$	$1.5\times10^{-4}e/\sqrt{\mathrm{Hz}}$	$7.6\times10^{-6}e/\sqrt{\mathrm{Hz}}$	$4.0\times10^{-5}e/\sqrt{\mathrm{Hz}}$
δq measured	$3.8\times10^{-5}e/\sqrt{\mathrm{Hz}}$	$4.7\times10^{-5}e/\sqrt{\mathrm{Hz}}$	$6.4\times10^{-6}e/\sqrt{\mathrm{Hz}}$	$1.86\times10^{-5}e/\sqrt{\mathrm{Hz}}$

[a]Reference 1.
[b]Reference 9.
[c]Reference 28.

mentally. Nevertheless, Eq. (27) provides a rather realistic estimate for the limiting charge sensitivity due to the first stage (HEMT) amplifier.

In practice, when a typical RF-SET made of Al is operated in the superconducting state, the SET seems to present three to four times better charge sensitive than in the normal state.[1,9]

VII. CONCLUSION

We have performed measurements on aluminum and multiwalled carbon nanotube RF-SETs and analyzed the results carefully. We have developed a detailed noise model, based on scattering matrix and noise wave formalisms. The signal-to-noise ratios obtained from our model agree well with the measured charge sensitivities. Our formulation also gives a recipe to extract noise parameters of the amplifier setup and the parasitic components of the impedance transformer. It is found that, in our setup, the first stage HEMT amplifier is the most inadequate component contributing nearly all of the charge noise.

Our noise analysis yields a general signal-to-noise ratio formula (18) that provides the basis for the estimation of sensitivities in RF-SET systems. Using Eq. (18), we calculated numerically the sensitivity of a RF-SET setup with a perfect impedance transformer over a wide range of parameter values. The results were compressed into a single phenomenological formula, Eq. (27), that may be used to estimate charge sensitivity of a typical metallic normal-state RF-SET.

As a final conclusion, if one wants to enhance the sensitivity of present-day RF-SET setups considerably, the noise temperature of the first (HEMT) amplifier after the SET should be lowered and the SET charging energy should be increased. From Eq. (27) one notices how high charging energy has major importance due to two facts. It allows a larger ac voltage amplitude over the SET and it leads to a lower normalized temperature t, which heating effects prevent in smaller charging energy SETs.

ACKNOWLEDGMENTS

The authors would like to thank Mikko Kiviranta and Mikko Paalanen for useful discussions. This work was supported by the Academy of Finland, by TEKES, and by the Large Scale Installation Program ULTI-III of the European Union (HPRI-1999-CT-00050). One of the authors (R.J.S.) would like to acknowledge funding from The David and Lucile Packard Foundation, and NASA Grant No. NAG5-11425. One of the authors (P.D.) would like to acknowledge funding from The Wallenberg Foundation.

APPENDIX A: *S*-MATRIX REPRESENTATION OF THE IMPEDANCE TRANSFORMER

In this section we write down explicitely the S matrix of a network of lumped element inductances, capacitances, and resistances. The impedance transformer of RF-SET may be viewed as two impedances Z_1 (the surface mount inductor with its parasitic elements) and Z_2 (the self-capacitance of a bonding pad):

$$Z_1 = j\omega L \| (R + 1/j\omega C_1), \tag{A1}$$

$$Z_2 = \frac{1}{j\omega C_2}, \tag{A2}$$

as illustrated in Fig. 17(a).

The transformation from impedances Z_1 and Z_2 to the S-matrix representation is given by

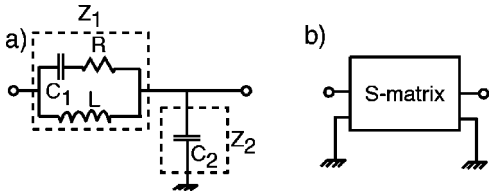

FIG. 17. (a) Lumped-element representation of LC matching circuit. Impedances Z_1 and Z_2 represent the total impedance of the corresponding dashed boxes. (b) Equivalent S-matrix representation.

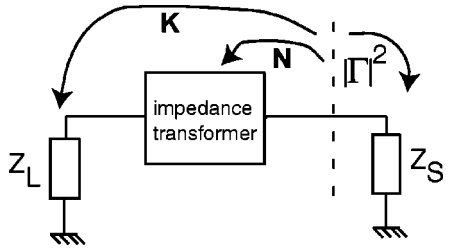

FIG. 18. Power transfer between the impedance transformer and the source impedance (N) and between the load impedance and the source impedance (K).

$$S_{11}=\frac{Z_1/Z_2+Z_1/Z_0-Z_0/Z_2}{2+Z_1/Z_2+Z_1/Z_0+Z_0/Z_2}, \tag{A3}$$

$$S_{12}=\frac{2}{2+Z_1/Z_2+Z_1/Z_0+Z_0/Z_2}, \tag{A4}$$

$$S_{21}=\frac{2}{2+Z_1/Z_2+Z_1/Z_0+Z_0/Z_2}, \tag{A5}$$

$$S_{22}=\frac{-Z_1/Z_2+Z_1/Z_0-Z_0/Z_2}{2+Z_1/Z_2+Z_1/Z_0+Z_0/Z_2}, \tag{A6}$$

where Z_0 is the characteristic impedance by which the S matrix is normalized.

APPENDIX B: POWER TRANSFER BETWEEN AMPLIFIER, IMPEDANCE TRANSFORMER, AND SET

In order to understand how power is transferred in the circuit we consider a situation illustrated in Fig. 18. We have a source impedance Z_S (amplifier, 50 Ω), a matching network at temperature T_m (the impedance transformer) described by its S parameters, and a load impedance Z_L (SET) at temperature T_L. We define constants K (N) as coupling of available power between Z_S and Z_L (Z_S and impedance transformer). A constant equal to 1 means that all available power is coupled between the objects. The available power that is coupled neither to Z_L nor to the impedance transformer is reflected back. Thus, we have an equation for the reflection constant Γ:

$$|\Gamma|^2+N+K=1. \tag{B1}$$

We define the power gain G as

$$G\equiv\frac{K}{N+K}. \tag{B2}$$

This is the ratio of the power coupled to the load to the total power that was not reflected back. Note that this gain is less than 1 in the analysis of this article. By using Eq. (5.84) from Ref. 18, we find an expression for the power gain

$$G=\frac{|S_{21}|^2(1-|\Gamma_l|^2)}{|1-S_{22}\Gamma_l|^2(1-|\Gamma_{in}|^2)}, \tag{B3}$$

where

$$\Gamma_l=\frac{Z_l-Z_0}{Z_l+Z_0}, \quad \Gamma_{in}=S_{11}+\frac{S_{12}S_{21}\Gamma_l}{1-S_{22}\Gamma_l}. \tag{B4}$$

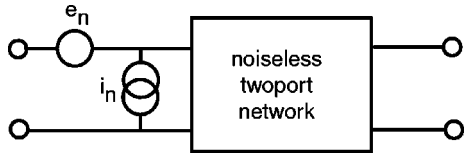

FIG. 19. Traditional way to represent noise of a two-port network.

By using Ref. 18 [Eq. (5.83)], we find K, the fraction of available power that is coupled to the load:

$$K=\frac{Z_s}{Z_0}\frac{|S_{21}^2(1-|\Gamma_l|^2)|1-\Gamma_s|^2}{|1-S_{22}\Gamma_l|^2|1-\Gamma_s\Gamma_{in}|^2}, \tag{B5}$$

where

$$\Gamma_s=\frac{Z_s-Z_0}{Z_s+Z_0}. \tag{B6}$$

If $Z_s=Z_0$ then $\Gamma_s=0$ and we find a shorter expression for K:

$$K=\frac{|S_{21}^2(1-|\Gamma_l|^2)|}{|1-S_{22}\Gamma_l|^2}. \tag{B7}$$

Using Eq. (B3), we can express N in terms of K and G:

$$N=\frac{K-GK}{G}. \tag{B8}$$

The above analysis allows us to calculate N and K from the knowledge of the S matrix of the coupling network, and the load and source impedances.

APPENDIX C: NOISE WAVE DESCRIPTION OF AN AMPLIFIER

Linear, noisy two-port networks are *traditionally* described by a voltage and a current noise generator and by their correlation at the input of a noiseless network, as illustrated in Fig. 19.[29] Following Ref. 30, we define quantities

$$R_n=\frac{\overline{|e_n|^2}}{4k_BT\Delta f}, \tag{C1}$$

$$g_n=\frac{\overline{|i_n|^2}}{4k_BT\Delta f}, \tag{C2}$$

and the correlation coefficient

$$\rho=\frac{\overline{i_ne_n^*}}{\sqrt{|e_n|^2|i_n|^2}}. \tag{C3}$$

Using these quantities one arrives at the usual formula for the noise figure:

$$F=F_{\text{emin}}+\frac{g_n}{R_s}|Z_s-Z_{\text{SOF}}|^2, \tag{C4}$$

where Z_s is the input impedance the two-port network sees, and $Z_{\text{SOF}}=R_{\text{SOF}}+jX_{\text{SOF}}$ is the input impedance that minimizes the noise figure (*source optimum* with respect to the noise *factor*). The optimum values for source impedance minimizing the noise figure are

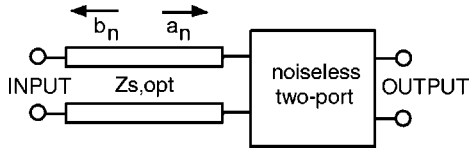

FIG. 20. Noise wave representation with two uncorrelated noise waves.

$$|Z_{\mathrm{SOF}}|^2=\frac{R_n}{g_n}, \tag{C5}$$

$$X_{\mathrm{SOF}}=\sqrt{\frac{R_n}{g_n}}\,\mathrm{Im}\,\rho. \tag{C6}$$

By defining noise wave generators

$$a_n=-\frac{e_n+Z_{\mathrm{SOF}}i_n}{2\sqrt{|\mathrm{Re}\,Z_{\mathrm{SOF}}|}}, \tag{C7}$$

$$b_n=\frac{e_n-Z_{\mathrm{SOF}}^*i_n}{2\sqrt{|\mathrm{Re}\,Z_{\mathrm{SOF}}|}}, \tag{C8}$$

describing a noise wave traveling towards the amplifier input (a_n) and a noise wave leaving the amplifier input (b_n), as illustrated in Fig. 20, one can have two uncorrelated noise waves *if* they travel in a transmission line with complex characteristic impedance Z_{SOF} in the amplifier input. This transformation transforms two noise sources with any correlation into two uncorrelated waves by using a transmission line with proper complex impedance.

In practice, however, we do not have a transmission line with a characteristic impedance Z_{SOF} at the input of an amplifier. Then, the transformation of Eqs. (C7) and (C8) cannot be employed to uncorrelate the power waves. It is convenient to define a pair of correlated noise waves traveling in the transmission line with characteristic impedance Z_0 denoted by A_n and B_n, as illustrated in Fig. 21.[31] Thus, A_{ns}, the total noise wave due to the amplifier at the amplifier input can be written in the form

$$A_{ns}=A_n+\Gamma B_n, \tag{C9}$$

and the measurable noise power becomes

$$\overline{|A_{ns}|^2}=\overline{|A_n|^2}+|\Gamma|^2\overline{|B_n|^2}+2\,\mathrm{Re}\{\Gamma\overline{A_n^*B_n}\}. \tag{C10}$$

We see that the correlation term in this noise power depends on the phase of Γ_s.

Often in low-temperature devices, the first stage amplifier is a balanced one.[32] For the *ideal* balanced amplifier the total noise wave is only a function of the magnitude of Γ, not the phase.[33] This means that the total noise can be written in the form

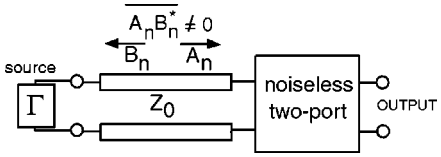

FIG. 21. Noise wave representation with two correlated noise waves. The source impedance is denoted by its reflection coefficient Γ.

TABLE IV. Extracted Rothe–Dahlke noise parameters for our amplifier system including all the components from the output of the impedance transformer up to the output of the last warm amplifier (see Fig. 4).

F_{emin}	g_n	Z_{SOF}
1.013	0.076 mS	56.17-j 4.22 Ω

$$\overline{|A_{ns}|^2}=\overline{|A_n|^2}+|\Gamma|^2\overline{|B_n|^2}. \tag{C11}$$

Generally, the question is how *balanced* the amplifier is. In practice, the measured noise power contains some correlation term that depends on both the linear magnitude and the phase of Γ.

APPENDIX D: EXTRACTION OF NOISE PARAMETERS

T-noise parameters may be transformed to the usual F_{emin}, g_n, and Z_{SOF} parameters using the identities[19]

$$F_{\mathrm{emin}}=1+\frac{1}{2T_r}[(T_\alpha-T_\beta)+\sqrt{(T_\alpha+T_\beta)^2-4T_\gamma^2}], \tag{D1}$$

$$g_n=\frac{T_\alpha+T_\beta-2T_\gamma\cos\phi_\gamma}{4T_r|\mathrm{Re}\{Z_0\}|}, \tag{D2}$$

$$Z_{\mathrm{SOF}}=|\mathrm{Re}\{Z_0\}|\frac{\sqrt{(T_\alpha+T_\beta)^2-4T_\gamma^2}}{T_\alpha+T_\beta-2T_\gamma\cos\phi_\gamma}+j\left(\mathrm{Im}\{Z_0\}-\frac{2T_\gamma\mathrm{Re}\{Z_0\}\sin\phi_\gamma}{T_\alpha+T_\beta-2T_\gamma\cos\phi_\gamma}\right), \tag{D3}$$

where Z_0 is an arbitrary complex reference impedance at the input port (usually, 50 Ω). Table IV displays the parameter values that are obtained for our amplifier setup from Eqs. (D1), (D2), and (D3) using the T parameters of Table 3.

The definition for extended noise factor F_e using T-noise parameters is given by[19]

$$F_e=1+\frac{T_\alpha+|\Gamma|^2T_\beta-2|\Gamma|T_\gamma\cos(\phi_S+\phi_\gamma)}{T_r(1-|\Gamma|^2)}, \tag{D4}$$

where $T_r=290$ K is the standard reference temperature for noise. The effective extended noise temperature $T_{\mathrm{ee}}=(F_e-1)290$ K of the amplifier system in Fig. 4(b) is illustrated in Fig. 22 as a function of source impedance Z_s.

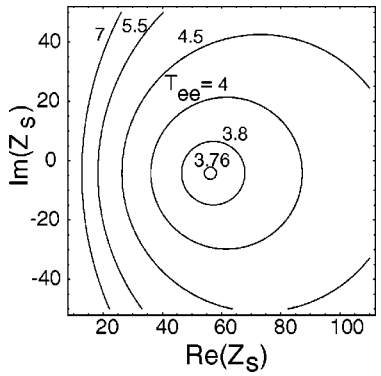

FIG. 22. Effective extended noise temperature T_{ee} of the employed HEMT amplifier as a function of source impedance Z_s. The contours denote T_{ee} = constant in kelvins.

[1] R. J. Schoelkopf, P. Wahlgren, A. A. Kozhevnikov, P. Delsing, and D. E. Prober, Science **280**, 1238 (1998).
[2] B. E. Kane, N. S. McAlpine, A. S. Dzurak, R. G. Clark, G. J. Milburn, H. B. Sun, and H. Wiseman, Phys. Rev. B **61**, 2961 (2000).
[3] V. Bouchiat, G. Chardin, M. H. Devoret, and D. Esteve, Hyperfine Interact. **109**, 345 (1997).
[4] M. P. Blencowe and M. N. Wybourne, Appl. Phys. Lett. **77**, 3845 (2000).
[5] A. N. Cleland, D. Esteve, C. Urbina, and M. H. Devoret, Appl. Phys. Lett. **61**, 2820 (1992).
[6] R. J. Schoelkopf, S. H. Moseley, C. M. Stahle, P. Wahlgren, and P. Delsing, IEEE Trans. Appl. Supercond. **9**, 2935 (1999).
[7] S. Komiyama, O. Astaflev, V. Antonov, T. Kutsuwa, and H. Hirai, Nature (London) **403**, 405 (2000).
[8] O. Astafiev, S. Komiyama, T. Kutsuwa, V. Antonov, Y. Kawaguchi, and K. Hirakawa, Appl. Phys. Lett. **80**, 4250 (2002).
[9] A. Aassime, D. Gunnarsson, K. Bladh, P. Delsing, and R. Schoelkopf, Appl. Phys. Lett. **79**, 4031 (2001).
[10] M.-O. André, M. Mück, J. Clarke, J. Gail, and C. Heiden, Appl. Phys. Lett. **75**, 698 (1999).
[11] P. Wahlgren, Ph.D. thesis, Chalmers University of Technology (1998).
[12] K. K. Likharev, Proc. IEEE **87**, 606 (1999).
[13] V. Bouchiat, Ph.D. thesis, CEA-Saclay (1997).
[14] S. Pohlen, Ph.D. thesis, Harvard University, Cambridge, MA (1999).
[15] J. Pettersson, P. Wahlgren, P. Delsing, D. B. Haviland, T. Claeson, N. Rorsman, and H. Zirath, Phys. Rev. B **53**, R13272 (1996).
[16] A. Aassime, G. Johansson, G. Wendin, R. J. Schoelkopf, and P. Delsing, Phys. Rev. Lett. **86**, 3376 (2001).
[17] T. Fujisawa and Y. Hirayama, Appl. Phys. Lett. **77**, 543 (2000).
[18] D. M. Pozar, *Microwave Engineering*, 1st ed. (Addison-Wesley, New York, 1990).
[19] J. Engberg and T. Larsen, *Noise Theory of Linear and Nonlinear Circuits* (Wiley, New York, 1995).
[20] S. Haykin, *An Introduction to Analog and Digital Communications*, 1st ed. (Wiley, New York 1989).
[21] D. Rogovin and D. J. Scalapino, Ann. Phys. **86**, 1 (1974).
[22] R. F. Bradley, Nucl. Phys. B **72**, 137 (1999).
[23] A. Fukushima, A. Sato, A. Iwasa, Y. Nakamura, T. Komatsuzaki, and Y. Sakamoto, IEEE Trans. Instrum. Meas. **46**, 289 (1997).
[24] D. V. Averin and K. K. Likharev, in *Mesoscopic Phenomena in Solids*, edited by B. L. Altshuler, P. A. Lee, and R. A. Webb (Elsevier, New York 1991), p. 173.
[25] A. N. Korotkov and M. A. Paalanen, Appl. Phys. Lett. **74**, 4052 (1999).
[26] R. J. Schoelkopf and M. H. Devoret, Nature (London) **406**, 1039 (2000).
[27] R. L. Kautz, G. Zimmerli, and J. M. Martinis, J. Appl. Phys. **73**, 2386 (1993).
[28] L. Roschier *et al.* (unpublished).
[29] H. Rothe and W. Dahlke, Proc. IRE **44**, 811 (1956).
[30] P. Penfield, IRE Trans. Circuit Theory **CT-9**, 84 (1962).
[31] R. P. Meyes, IEEE Trans. Microwave Theory Tech. **MTT-26**, 34 (1978).
[32] K. Kurokawa, Bell Syst. Tech. J. **44**, 1675 (1965).
[33] A. R. Kerr, IEEE Microw. Guid. Wave Lett. **8**, 390 (1998).